

Confinement of the Sun's interior magnetic field: some exact boundary-layer solutions

T. S. Wood and M. E. McIntyre

Department of Applied Mathematics and Theoretical Physics, University of Cambridge;
www.damtp.cam.ac.uk/user/tsw25/ and www.atm.damtp.cam.ac.uk/people/mem/

Abstract. High-latitude laminar confinement of the interior field \mathbf{B}_i is shown to be possible. Mean downwelling U as weak as $2 \times 10^{-6} \text{ cm s}^{-1}$ – gyroscopically pumped by turbulent stresses in the overlying convection zone and/or tachocline – can hold the field in advective–diffusive balance within a confinement layer of thickness scale $\delta \sim 1.5 \text{ Mm} \sim 0.002 R_\odot$. The confinement layer sits at the base of the high-latitude tachocline, near the top of the radiative envelope and just above the ‘tachopause’ marking the top of the helium settling layer. A family of exact, laminar, frictionless, axisymmetric confinement-layer solutions is obtained in cylindrical polar coordinates, for uniform downwelling in the limit of strong rotation Ω_i and stratification N . The downwelling cannot penetrate the helium layer and must therefore feed into an equatorward flow immediately above the tachopause. The retrograde Coriolis force on that flow is balanced by a prograde Lorentz force within the confinement layer. Buoyancy forces keep the tachopause approximately horizontal. For typical solar N values $\sim 10^{-3} \text{ s}^{-1}$ this type of dynamics holds over a substantial range of colatitudes, e.g. nearly out to colatitude 40° when $U \lesssim 10^{-5} \text{ cm s}^{-1}$ for modest $|\mathbf{B}_i|$ values \sim tens of gauss.

The angular-momentum budget implied by the downwelling and equatorward flow, importing low and exporting high angular momentum, dictates that the confinement layer must exert a net retrograde torque on its surroundings through laminar Maxwell stresses. Some of that torque is exerted downward through the tachopause upon the interior, against the Ferraro constraint, and the rest is exerted across the periphery of the confinement layer at some outer colatitude $\lesssim 40^\circ$. The profiles of velocity and magnetic field within the confinement layer are fixed by two external conditions, first the partitioning of the torque between the contributions exerted on the interior and across the periphery, and second the vertical profile of Maxwell stress at the periphery. In default of detailed models of what happens near the periphery, we provisionally suggest that a natural simplest choice of model would be one in which all the net torque is exerted on the interior.

Keywords: Sun's differential rotation, solar tachocline, interior magnetic field confinement, Ferraro constraint, helium settling layer, helium diffusion layer

PACS: 96.60.Jw

INTRODUCTION

The near-rigid rotation $\Omega_i = 2.7 \times 10^{-6} \text{ rad s}^{-1}$ observed in the Sun's interior can be most credibly explained via the Ferraro constraint from a confined global-scale interior magnetic field \mathbf{B}_i (Gough & McIntyre 1998, hereafter GM98); also McIntyre (1994–2007). For stability \mathbf{B}_i must have comparable toroidal and poloidal components (e.g. Braithwaite & Spruit 2004). \mathbf{B}_i could be axisymmetric and aligned with the Sun's rotation axis as proposed in GM98, or oblique as is typical of Ap stars. We focus on the aligned case as presenting, in some ways, the greatest problems.

The main problem, previously addressed by Garaud (2002–08) and by Brun & Zahn (2006), is how to confine \mathbf{B}_i at the pole and in high latitudes. It is necessary to stop the poloidal field from diffusing up through the polar caps and thereby imposing the convection zone's high-latitude differential rotation upon the interior. Such differential rotation conflicts with the helioseismic evidence.

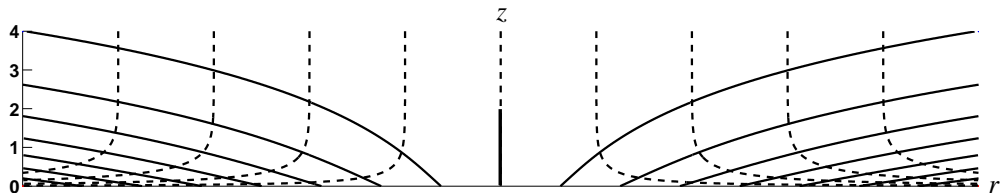


FIGURE 1. Streamlines of the downwelling flow \mathbf{u} (dashed curves) and of the poloidal part of \mathbf{B} (solid curves), spacing arbitrary. The horizontal axis is colatitude in arbitrary units, measured from the central symmetry axis or rotation axis. The vertical axis is heliopotential altitude, or radial increment, z , in units of δ . Although there is a field line on the central symmetry axis, as well as a streamline, the strength of the field decays like $\exp(-z/\delta)$ with altitude z . The downwelling profile $u_z(z) = -U[1 - \exp(-3z/\delta)]$.

Following GM98 we propose that \mathbf{B}_i is confined to the interior, in high latitudes, via a frictionless laminar boundary layer at the base of the stably stratified tachocline. The confinement is brought about by weak downwelling of magnitude U , say, taken to be a persistent feature of the mean meridional circulations (MMCs) in the lower tachocline. Such downwelling is to be expected from the ‘gyroscopic pumping’ caused by turbulent Reynolds and Maxwell stresses in the overlying layers (McIntyre 2007), in the same way that Ekman pumping is caused by ordinary viscous stresses.

The overlying turbulent layers consist of the convection zone and possibly also the tachocline (Spruit 2002). There are uncertainties in how to characterize those turbulent layers in detail. But because of the ‘antifrictional’ sense of the convection zone’s turbulent stresses – driving it retrogradely relative to the interior in high latitudes – there should be a systematic tendency, by one means or another, for the gyroscopic pumping to produce downwelling above the top of the radiative envelope in high latitudes. One possible such scenario is discussed in McIntyre (2007), following Spruit (2002). There the gyroscopic pumping is, in fact, a case of ordinary Ekman pumping near the bottom of an MHD-turbulent tachocline.

We assume that the bulk of the radiative envelope beneath is itself locked into rigid rotation Ω_i with the help of the Ferraro constraint from \mathbf{B}_i , and that gravitational settling has produced molecular-weight gradients in the form of a helium settling layer in the outer 50–100Mm or so. Such a helium layer is a feature of standard solar models (e.g. Ciaccio et al. 1997). Its existence is indicated also by the helioseismic evidence, despite current uncertainties about heavy-element abundances and their effects on opacity (e.g. Christensen-Dalsgaard & Di Mauro 2007).

The helium diffusivity is tiny, $\sim 10\text{cm}^2\text{s}^{-1}$, in comparison with the thermal and magnetic diffusivities $\kappa \sim 10^7\text{cm}^2\text{s}^{-1}$ and $\eta \sim 3 \times 10^2\text{cm}^2\text{s}^{-1}$ (e.g. Gough 2007). Therefore the helium layer is nearly impervious to MMCs. Mestel & Moss (1986) call this the ‘ μ -choke’ or ‘ μ -barrier’ effect; see also Mestel (1953). The high-latitude downwelling, whatever its origin, must therefore feed into an equatorward flow just above the ‘tachopause’ marking the top of the helium layer. The retrograde Coriolis force on that equatorward flow needs to be balanced by a prograde Lorentz force. Buoyancy forces from the stable stratification keep the tachopause and the helium layer beneath it very close to the horizontal, along with the stratification surfaces themselves (McIntyre 2007, §8.5). We report a new family of exact steady solutions of the nonlinear equations showing how all these elements fit together, confining \mathbf{B}_i within a layer of thickness scale $\delta = \eta/U$ while transmitting a retrograde torque to the interior.

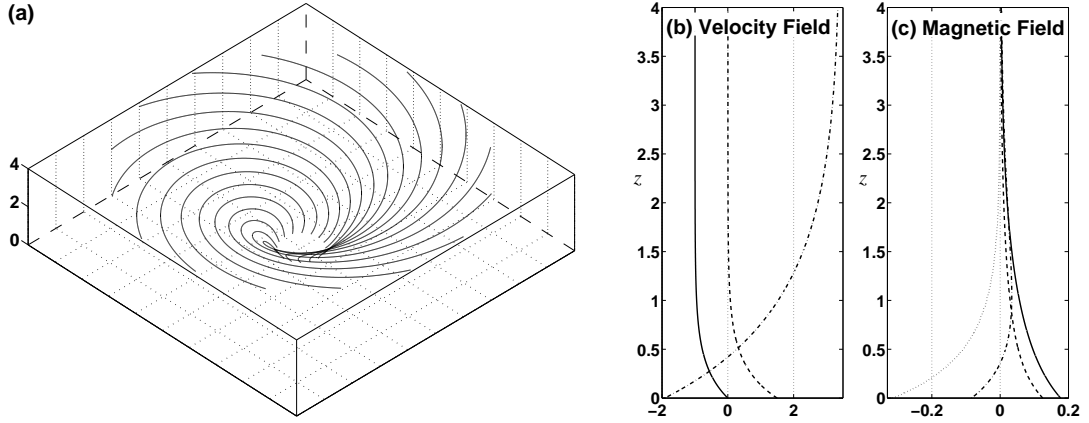


FIGURE 2. Further views of the same solution. The view (a) of field lines shows only those lines that emerge from the tachopause at a single colatitude near the pole. The lines emerging at other colatitudes have the same shape dilated horizontally (see text). The profiles (b) are those of u_z (solid), u_r (dashed) and u_ϕ (dot-dashed), in units of U , Ur/δ and $50Ur/\delta$ respectively; (c) are B_z (solid), B_r (dashed), B_ϕ (dot-dashed), and the auxiliary function \hat{B}_ϕ (dotted), in units of $(\eta\Omega_i)^{1/2}$ for B_z and $(\eta\Omega_i)^{1/2}r/\delta$ for the rest. The shape of $\hat{u}_\phi(z)$, not shown in (b), is nearly indistinguishable from $u_\phi(z) - u_\phi(\infty)$. See (4)–(9) below.

CONFINEMENT-LAYER SOLUTIONS

The confinement-layer solutions are axisymmetric similarity solutions obtained in cylindrical polar coordinates (r, ϕ, z) and valid in some region surrounding the pole, for any finite stratification N . Figure 1 shows an example, with the north pole at the centre. The z axis is central, pointing upward, and z measures altitude in units of δ . The cylindrical radial coordinate r is proportional to colatitude and is in arbitrary units, the structure being self-similar under radial dilatation. The similarity solutions have vertical field components u_z and B_z that are independent of r , and horizontal components u_r , u_ϕ and B_r , B_ϕ proportional to r . Because $\nabla \cdot \mathbf{B} = 0$ we have $2B_r = -B'_z r$ where the prime denotes $\partial/\partial z$. We assume anelastic flow with $\delta \ll$ pressure scale height (60 Mm or more), so that background density is constant (Boussinesq limit) and $\nabla \cdot \mathbf{u} = 0$, implying $2u_r = -u'_z r$.

The boundary conditions include continuity of \mathbf{B} at the tachopause $z = 0$. The magnetic field \mathbf{B}_i just beneath the tachopause therefore has a matching similarity structure. The simplest such field has $B_{ir} = B_{i0}r$ and $B_{iz} = -2B_{i0}z + C_i$, where B_{i0} and C_i are constants, so that $\nabla \cdot \mathbf{B}_i = 0$, while the azimuthal component $B_{i\phi}$ is taken $\propto B_{iz}r$ to ensure the vanishing of the interior's azimuthal Lorentz force, right-hand side of (3) hereunder. Figure 2 shows further views of the same solution. The equations solved are

$$\eta B''_z = B'_z u_z - B_z u'_z \quad (1)$$

$$\eta B''_\phi = B'_\phi u_z - B_z u'_\phi \quad (2)$$

$$2\Omega_i u_r = -\Omega_i u'_z r = B_z B'_\phi - B'_z B_\phi = B_z^2 (B_\phi/B_z)' \quad (3)$$

of which the first two come from the induction equation after substituting the similarity structure into $\nabla \times (\mathbf{u} \times \mathbf{B})$, and the third from the azimuthal momentum equation in the limit of small Rossby number, thus retaining only Coriolis and not relative accelerations; \mathbf{B} is in units of Alfvén speed, $\sim \frac{1}{2} \text{cm s}^{-1}$ per gauss at tachocline mass densities. The η terms are exact because the similarity structure makes the horizontal derivatives vanish.

In the absence of specific information about the vertical profile of Maxwell stresses $B_r B_\phi$ at the periphery, there is an undetermined function of z in the problem. We may use this freedom to specify the vertical profile $u_z(z)$ of the downwelling. Then (1) becomes a linear problem for $B_z(z)$. It is solvable with $B_z'(0) = -2B_{i0}$ (matching the r components) and with $B_z(z)$ decaying like $\exp(-z/\delta)$ as $z \rightarrow \infty$. This determines both $B_z(z)$ and C_1 . Then, provided only that $|u_z|$ converges to U faster than $\exp(-2z/\delta)$, (3) has a solution

$$B_\phi = \hat{B}_\phi \equiv -2\Omega_i B_z \int_z^\infty \frac{u_r}{B_z^2} dz. \quad (4)$$

In the example shown in the figures we took $u_z = -U[1 - \exp(-3z/\delta)]$, which implies that $u_r = -\frac{1}{2}u_z' r = \frac{3}{2}(Ur/\delta)\exp(-3z/\delta)$, giving the \hat{B}_ϕ profile shown as the dotted, leftmost curve in Fig. 2c. Then (2) has a corresponding solution

$$u_\phi = \hat{u}_\phi \equiv \int_z^\infty \frac{\eta \hat{B}_\phi'' - u_z \hat{B}_\phi'}{B_z} dz. \quad (5)$$

Under our assumptions, both (4) and (5) are finite at $z = 0$, and are evanescent as $z \rightarrow \infty$, respectively like $\exp(-2z/\delta)$ and $\exp(-z/\delta)$ in the example shown. The foregoing procedure is robust and well-conditioned. In the simplest cases in which u_z and u_z' are both negative for all z , as in the figures, it is easy to see by inspection of (1), qualitatively integrating it downward from $z = \infty$, that B_z'' on the left and both terms on the right are positive for all z . It then follows from (4) that \hat{B}_ϕ is negative for all z . But \hat{u}_ϕ and \hat{u}_ϕ' can change sign, though in fact \hat{u}_ϕ is negative and monotonic in the example shown.

We still have a pair of undetermined parameters at our disposal because (2) and (3) are also satisfied, for any constants α and β , by

$$B_\phi = \hat{B}_\phi + \alpha B_z r \quad \text{and} \quad u_\phi = \hat{u}_\phi + (\alpha u_z + \beta) r. \quad (6)$$

Here (1) has been used to simplify the last term on the right. The α term in B_ϕ contributes nothing to the azimuthal Lorentz force on the right-hand side of (3), but does change the Maxwell stresses acting across the tachopause $z = 0$ and the periphery, $r = r_p$ say, by equal and opposite amounts. In other words α governs the partitioning of Maxwell torques between tachopause and periphery.

In the example shown α was chosen, purely on Occam's-razor grounds, to make the Maxwell torque on the periphery zero. Lacking information about conditions at the periphery, zero is arguably the simplest choice. The torque $\propto \int_0^\infty B_r B_\phi dz$. It is zero if

$$\alpha = - \frac{\int_0^\infty B_r \hat{B}_\phi dz}{\int_0^\infty B_r B_z r dz} = 1.31 \delta^{-1} \quad (7)$$

from the first of (6); the quotient is independent of r because of the similarity structure.

To find β we integrate (2) across the tachopause and use (3) to give

$$u_\phi(0) = -\Lambda^{-1} u_r(0) \quad (8)$$

where $\Lambda \equiv B_z^2(0)/(2\Omega_i \eta)$, the Elsasser number based on $B_z(0)$ ($\sim B_{i0} \delta$), determining the direction of the frictionless slip flow at the tachopause just above the rigidly-rotating interior. The slip flow is equatorward and retrograde, following a logarithmic spiral. For finite viscosity ν there would be a laminar Ekman layer of thickness scale $\delta_\nu \sim$

$(\nu/\Omega)^{1/2} \sim 3 \times 10^{-5} \text{Mm} \ll \delta$, if we take $\nu \sim 30 \text{cm}^2 \text{s}^{-1}$ (Gough 2007). Its flow is unobstructed by the field lines since magnetic diffusion on the scale δ_ν is almost instantaneous. Note (8) gives the spiral just *above* the Ekman layer. From (6) and (8),

$$\beta = -r^{-1} \hat{u}_\phi(0) - \Lambda^{-1} r^{-1} u_r(0) = 1.73 U \delta^{-1} \times 10^2. \quad (9)$$

In fact Λ^{-1} measures the spiralling of the field lines as well as that of the flow lines, because (4)–(9) imply the order-of-magnitude relations

$$B_\phi \sim \hat{B}_\phi \sim 2\Omega_i U r / B_z, \quad u_\phi \sim \hat{u}_\phi \sim U B_\phi / B_z, \quad (10)$$

and

$$B_\phi / B_r \sim u_\phi / u_r \sim \Lambda^{-1}. \quad (11)$$

Recall that $\delta = \eta/U$ and $2u_r = -u'_z r \sim U r / \delta$, $2B_r = -B'_z r \sim B_{i0} r$. The numerical factors implicit in (11) differ considerably from unity because of the disparity in vertical scales between $\exp(-z/\delta)$, $\exp(-2z/\delta)$ and $\exp(-3z/\delta)$, along with the peculiar balance of terms in (2) that enables \hat{B}_ϕ to evanesce faster than $\exp(-z/\delta)$. In the example shown in the figures, $\Lambda = 1.57 \times 10^{-2}$. Fig. 2 shows that $|B_\phi/B_r|$ attains values considerably smaller numerically, and $|u_\phi/u_r|$ distinctly larger, than $\Lambda^{-1} \approx 60$.

By contrast with GM98's thermomagnetic boundary layer, whose dynamics crucially involved the tilting of stratification surfaces, our exact solutions of (1)–(3) impose no restriction on U values and mass throughput for given B_{i0} . However, there is an implicit restriction, for given peripheral radius $r = r_p$ and stratification N . N has been assumed strong enough to hold stratification surfaces horizontal. Only then can the uniform downwelling satisfy the thermal diffusion equation, displacing the stratification surfaces vertically without tilting them. A scale analysis, omitted for brevity, shows that the tilting becomes noticeable at the periphery if in order of magnitude

$$U \sim U_{\text{crit}} \equiv \min \left[(a B_{i0} / r_p)^{1/3}, b (B_{i0} r_p)^{-1} \right] \quad (12)$$

where $a = 0.4(\eta/\kappa)^{1/2}(\eta^2 N / \Omega_i) \sim 0.7 \times 10^5 \text{cm}^4 \text{s}^{-2}$ and $b = 0.1(\eta/\kappa)^{1/2} \eta N \sim 0.15 \times 10^{-3} \text{cm}^2 \text{s}^{-2}$. The min function arises from the azimuthal vorticity balance. In the strong-field case (second argument, roughly corresponding to $\Lambda \gtrsim 1$), the tilting of the stratification surfaces is balanced solely by a Lorentz force-curl. In the weak-field case (first argument, $\Lambda \lesssim 1$) there is an additional contribution from vortex twisting $2\Omega_i u'_\phi$. The crossover corresponds to $B_{i0} r_p \sim 15 \text{cm s}^{-1}$ ($\sim 30\text{G}$) when $r_p = 350 \text{Mm}$, i.e. to $|\mathbf{B}_i| \sim 30\text{G}$ near an outer colatitude $\sim 40^\circ$. Then $U_{\text{crit}} \sim 10^{-5} \text{cm s}^{-1}$.

The Rossby number $\mathcal{R} = \max |r^{-1} \mathbf{u} \cdot \nabla (r u_\phi) / (2\Omega_i u_r)| \sim (U/B_z(0))^2 \sim U^4 / (\eta B_{i0})^2$, $\lesssim 10^{-6}$ at crossover if $U \lesssim U_{\text{crit}}$, and similarly small throughout the parameter range of interest, strongly justifying our use of the small- \mathcal{R} limit. Inverse gradient Richardson numbers $|\mathbf{u}'|^2 / N^2 \sim (U/U_{\text{crit}})(\eta/\kappa)\mathcal{R}$ in the confinement layer, and $\sim (U/U_{\text{crit}})(\eta/\kappa)\mathcal{R}(\delta/\delta_\nu)^2 \sim (U/U_{\text{crit}})(\eta/\kappa)U^2 \Omega_i / (\nu B_{i0}^2)$ in the Ekman slip layer, respectively $\lesssim 10^{-11}$ and $\lesssim 10^{-3}$ at crossover. So the flows are strongly shear-stable.

Spruit (1999) shows that in stably stratified shear flows the first MHD instabilities to kick in will be diffusion-mediated Tayler kink or tipping instabilities of B_ϕ . In the weak-field case $\Lambda \lesssim 1$ (the most vulnerable, with strong spiralling) we find Tayler stability for $U \lesssim (B_{i0}/B_{i0\text{crossover}})^{1/6} U_{\text{crit}}$. Stability increases further when $\Lambda \gtrsim 1$. So

the solutions probably represent real laminar flows.

CONCLUDING REMARKS

The suggestion in (12) of a limiting mass flow and therefore, by implication, of an upper bound on the torque transmissible to the interior, is no more than a suggestion at present. However, the scaling leading to (12) does have points of similarity to the scaling governing the mass-flow-limited thermomagnetic boundary layer proposed in GM98. A peripheral thermomagnetic boundary layer might impose a mass-flow limit. Such a limit would have implications, in turn, for the possible range of interior field strengths $|\mathbf{B}_i|$. In particular, the steep falloff of U_{crit} on the strong-field side of (12) suggests a sharp upper bound on confinable $|\mathbf{B}_i|$ strengths.

A mass-flow limit, if confirmed, would also bear on the question of whether a Tayler–Spruit dynamo can run continuously or intermittently in the tachocline above the confinement layer (McIntyre 2007, §8.4). That question is critical to associated questions about deep tachocline ventilation and lithium burning.

ACKNOWLEDGMENTS

We thank Jørgen Christensen-Dalsgaard, Werner Däppen, Scilla Degl’Innocenti, Pascale Garaud, Douglas Gough, Mark Miesch, Steven Shore, and Mike Thompson for helpful comments. TSW is supported by a Research Studentship from the Science and Technology Facilities Council.

REFERENCES

- Braithwaite J., Spruit H. C., 2004, *Nat*, 431, 819
Brun A. S., Zahn J.-P., 2006, *A&A*, 457, 665
Ciaccio F., Degl’Innocenti S., Ricci B., 1997: *A&A*, 123, 449
Christensen-Dalsgaard J., Di Mauro M. P., 2007, in Straka C. W., Lebreton Y., Monteiro M. J. P. F. G., eds, *Stellar Evolution and Seismic Tools for Asteroseismology – Diffusive Processes in Stars and Seismic Analysis*. EAS Publ. Ser. 26, EDP Sciences, Les Ulis, France, DOI: 10.1051/eas:2007121
Garaud P., 2002, *MNRAS*, 329, 1
Garaud P., 2003, in Thompson M. J., Christensen-Dalsgaard, J., eds, *Stellar Astrophysical Fluid Dynamics*. Cambridge University Press, Cambridge
Garaud P., 2007, in Hughes D. W., Rosner R., Weiss N. O., eds, *The Solar Tachocline*. Cambridge University Press, Cambridge
Garaud P., 2008, *this Proceedings*.
Gough D. O., 2007, in Hughes D. W., Rosner R., Weiss N. O., eds, *The Solar Tachocline*. Cambridge University Press, Cambridge
Gough D. O., McIntyre M. E., 1998, *Nat*, 394, 755
McIntyre M. E., 1994, in E. Nesme-Ribes, ed, *The Solar Engine and its Influence on the Terrestrial Atmosphere and Climate* (Vol. 25 of NATO ASI Subseries I, Global Environmental Change), Springer-Verlag, Heidelberg
McIntyre M. E., 2003, in Thompson M. J., Christensen-Dalsgaard J., eds, *Stellar Astrophysical Fluid Dynamics*. Cambridge University Press, Cambridge
McIntyre M. E., 2007, in Hughes D. W., Rosner R., Weiss N. O., eds, *The Solar Tachocline*. Cambridge University Press, Cambridge
Mestel L., 1953, *MNRAS*, 113, 716
Mestel L., Moss D. L., 1986, *MNRAS*, 221, 25
Spruit H. C., 1999, *A&A*, 349, 189
Spruit H. C., 2002, *A&A*, 381, 923